Original Article | Cardiovascular Imaging

eISSN 2005-8330
https://doi.org/10.3348/kjr.2020.0001
Korean J Radiol 2021;22(4):513-524

Korean Journal of Radiology
KJR

Utility of Noncontrast Magnetic Resonance Angiography for Aneurysm Follow-Up and Detection of Endoleaks after Endovascular Aortic Repair

Hiroshi Kawada, MD[1], Satoshi Goshima, MD, PhD[1, 2], Kota Sakurai, MD[3], Yoshifumi Noda, MD[1], Kimihiro Kajita, RT[4], Yukichi Tanahashi, MD[1], Nobuyuki Kawai, MD[1], Narihiro Ishida, MD, PhD[5], Katsuya Shimabukuro, MD, PhD[5], Kiyoshi Doi, MD, PhD[5], Masayuki Matsuo, MD, PhD[1]

Departments of [1]Radiology, [4]Radiology Services, and [5]General and Cardiothoracic Surgery, Gifu University Hospital, Gifu, Japan; [2]Department of Diagnostic Radiology and Nuclear Medicine, Hamamatsu University School of Medicine, Hamamatsu, Japan; [3]Department of Radiology, Chuno Kosei Hospital, Seki, Japan

Objective: To assess the noncontrast two-dimensional single-shot balanced turbo-field-echo magnetic resonance angiography (b-TFE MRA) features of the abdominal aortic aneurysm (AAA) status following endovascular aneurysm repair (EVAR) and evaluate to detect endoleaks (ELs).

Materials and Methods: We examined four aortic stent-grafts in a phantom study to assess the degree of metallic artifacts. We enrolled 46 EVAR-treated patients with AAA and/or common iliac artery aneurysm who underwent both computed tomography angiography (CTA) and b-TFE MRA after EVAR. Vascular measurements on CTA and b-TFE MRA were compared, and signal intensity ratios (SIRs) of the aneurysmal sac were correlated with the size changes in the AAA after EVAR (AAA prognoses). Furthermore, we examined six feasible b-TFE MRA features for the assessment of ELs.

Results: There were robust intermodality (r = 0.92–0.99) correlations and interobserver (intraclass correlation coefficient = 0.97–0.99) agreement. No significant differences were noted between SIRs and aneurysm prognoses. Moreover, "mottled high-intensity" and "creeping high-intensity with the low-band rim" were recognized as significant imaging findings suspicious for the presence of ELs (p < 0.001), whereas "no signal black spot" and "layered high-intensity area" were determined as significant for the absence of ELs (p < 0.03). Based on the two positive features, sensitivity, specificity, and accuracy for the detection of ELs were 77.3%, 91.7%, and 84.8%, respectively. Furthermore, the k values (0.40–0.88) displayed moderate-to-almost perfect agreement.

Conclusion: Noncontrast MRA could be a promising imaging modality for ascertaining patient follow-up after EVAR.

Keywords: *Abdominal aortic aneurysm; Stents; Stent-graft; Magnetic resonance imaging; Computed tomography; Endoleak; b-TFE MRA*

INTRODUCTION

Nearly all randomized controlled trials have reported promising perioperative mortality and morbidity in patients undergoing endovascular aneurysm repair (EVAR) for abdominal aortic aneurysms (AAAs), making it a suitable substitute for conventional open repair (1-4). Although EVAR aims to evade the rupture of aneurysms by excluding the aneurysmal sac from the systemic circulation, long-term and procedure-related complications, including various types of endoleaks (ELs), stent-graft migration, and stent-graft kinking, are often reported after EVAR (5-7); hence,

Received: December 31, 2019 **Revised:** June 2, 2020 **Accepted:** June 22, 2020
Corresponding author: Satoshi Goshima, MD, PhD, Department of Diagnostic Radiology and Nuclear Medicine, Hamamatsu University School of Medicine, 1-20-1 Handayama, Higashi-ku, Hamamatsu, Shizuoka 431-3125, Japan.
• E-mail: gossy55555@gmail.com

guidelines recommend lifelong follow-up for monitoring these complications and the size of aneurysms (8-10).

In spite of using various imaging modalities for post-EVAR follow-up, contrast-enhanced computed tomography angiography (CTA) remains extensively used owing to its excellent reproducibility and spatial and/or contrast resolution, despite disadvantages, such as the related radiation exposure and potential for nephrotoxicity (11). Novel magnetic resonance (MR) imaging technologies facilitate obtaining high-quality noncontrast MR angiography (MRA) images, and the usefulness of these images for preoperative planning (12) and postoperative surveillance has been reported in a small case series (13). Therefore, we hypothesize that this approach could be beneficial for patients' post-EVAR follow-up. Hence, this study aimed to investigate the degree of metallic artifacts related to various stent-grafts in MRA images in a phantom study, and to assess the noncontrast MRA features of the AAA status after EVAR and evaluate its diagnostic performance to detect ELs in a clinical study.

MATERIALS AND METHODS

Study Design

This prospective study comprised both phantom and clinical studies and was approved by the Institutional Review Board of our institute. We obtained written informed consent regarding the use of clinical data from all patients (IRB No. 23-3). While we evaluated the degree of metal-induced susceptibility artifacts in MRA images in the phantom study, the clinical study compared the noncontrast-enhanced MRA features of anatomical structures post-EVAR and contrast-enhanced CTA. Furthermore, we assessed the imaging features and diagnostic performance of MRA to detect ELs post-EVAR.

Phantom Study

We used the following four different stent-grafts to conduct the phantom study: Zenith (Cook Medical; TFFB-28-111-ZT), Excluder (WL Gore & Associates; PXT-231216), Powerlink (Endologix; 22-13-120BL), and Endurant (Medtronic; ENBF28-16-166)—all commercially available in our country for EVAR. Briefly, we used a water-filled container and a stent-graft; the latter was fixed in a rectangular parallelepiped-shaped polypropylene container (17 x 24 x 9 cm) that was filled with water (Supplementary Fig. 1). Then, we obtained transaxial images perpendicular to the direction of the main body section for each stent-graft using the following MR imaging parameters: a respiratory-triggered two-dimensional single-shot balanced turbo-field-echo (b-TFE) sequence (Balanced TFE M2D, Philips Healthcare); repetition time (TR)/echo time (TE), 2.8/1.4 ms; flip angle 70°; matrix, 192 x 256 with 320 recon; field of view, 40 x 26 cm; slice thickness/overlap, 6/2 mm; and acquisition time, 5 minutes. Four abdominal and interventional radiologists and one radiological technologist (17-, 11-, 7-, 5-, and 15-year experience, respectively) independently measured stent-graft diameters after reaching consensus on the part to be measured, including artifacts, at three different slice levels using a multimodality workstation (GE Advantage Workstation 4.2; GE Healthcare). We averaged these values and generated an expansion ratio (ExR) using actual and calculated stent-graft diameters (ExRs = calculated diameter/actual diameter). Finally, we compared the values between different stent-grafts.

Clinical Study

Patients

In this study, we prospectively enrolled patients diagnosed with infrarenal AAA and/or common iliac artery aneurysm, from September 2011 to August 2013, and admitted to our hospital for elective EVAR and underwent both contrast-enhanced CTA and noncontrast MRA within 2 weeks post-EVAR.

CT Scan Protocol

We performed CT using a 64-channel scanner (Brilliance 64; Philips Healthcare) and obtained CT images during a single breath-hold event using a 64 x 0.625 mm collimation device (section thickness, 1.25 mm) with no intersectional gap and covering the abdominal aorta, internal and external iliac, and femoral arteries. Each scan was performed using the following parameters: gantry rotation time, 0.5 seconds; pitch, 0.80; and tube voltage, 120 kVp. In addition, we used automatic current selection in the z-axis (Dose-Right ACS, Philips Healthcare) to minimize the radiation dose, with a typical scanning time of 7–8 seconds. Next, multiplanar reformatted images were reconstructed in the coronal and sagittal planes (section thickness, 2.5 mm) with no intersectional gap. Notably, each patient had a 21-gauge intravenous catheter placed in an upper extremity vein (typically in an antecubital vein), and the scanning delay time was established using a bolus-tracking technique with an enhancement threshold of 100

https://doi.org/10.3348/kjr.2020.0001

Korean Journal of Radiology
KJR

Hounsfield unit measured over the lumen of the aorta at the level of the diaphragmatic dome. We administered all patients a nonionic iodinated contrast material (iopamidol 370; Bayer Healthcare) containing 370 mg iodine/mL, using a commercially available power injector (Dual Shot GX; Nemotokyorindo) at an injection rate of 4 mL/s followed by a 20-mL saline chaser (14). In the protocol, we switched the contrast medium injection to a saline chaser at the time of triggering. Hence, the total volume of the contrast material delivered was 60–96 mL (mean, 78 mL). Furthermore, we performed dual-phase scans at 5 seconds and 100 seconds after reaching the aortic threshold (15, 16).

MR Imaging Protocol

We performed noncontrast MRA using a 1.5T MR system (Intera Achieva Nova Dual 1.5T; Philips Healthcare) and a 16-channel phased-array body multicoil (SENSE XL Torso, Philips Healthcare). Next, MRA images were obtained using a respiratory-triggered two-dimensional single-shot b-TFE sequence (Balanced TFE M2D, Healthcare) in the transaxial (TR/TE, 2.8/1.39 ms; flip angle, 80°; matrix, 192 x 256; field of view, 40 x 26 cm; slice thickness/overlap, 6/2 mm; and acquisition time, 5 minutes), coronal (TR/TE, 2.9/1.43 ms; flip angle, 80°; matrix, 192 x 256; field of view, 40 x 36 cm; slice thickness/overlap, 7/3 mm; and acquisition time, 4 minutes), and sagittal (TR/TE, 2.6/1.31 ms; flip angle, 80°; matrix, 192 x 256; field of view, 40 x 36 cm; slice thickness/overlap, 7/3 mm; and acquisition time, 3 minutes) planes. Notably, we used the same transaxial plane parameters in both phantom and clinical studies.

Quantitative Analysis

Anatomical Measurements

Before blinding the anatomical measurements for accuracy, 3 unblinded authors, including 1 cardiovascular surgeon and 2 abdominal and interventional radiologists (with 24-, 17-, and 7-year experience, respectively), reviewed the CTA and MRA images of each patient. All the unblinded authors ascertained seven key anatomical structures for size measurements required for the post-EVAR follow-up, such as the infrarenal proximal landing position, distal iliac landing position, and aneurysmal sac size. Hence, under the unblinded authors' guidance, CTA and MRA were separately assessed by 2 independent observers (with 11- and 5-year experience in interventional radiological practice) using a DICOM viewer (ShadeQuest/ViewR; Yokogawa Medical Solutions). The measurements included were as follows: 1) aortic neck diameter in the stent-graft, 2) maximum minor axis diameter of an aneurysm, 3) maximum diameter of an aneurysm, 4) right iliac diameter in the stent-graft, 5) left iliac diameter in the stent-graft, 6) right iliac diameter distal to the stent-graft edge, and 7) left iliac diameter distal to the stent-graft edge (Fig. 1). We measured the diameters perpendicular to the central axis of the vessel using coronal or sagittal images.

Signal Intensity Ratio

We quantitatively evaluated the correlation between the size change of the aneurysmal sac after obtaining the MRA images and the signal intensity ratio (SIR) on noncontrast MRA images. The same 2 blinded observers measured the mean signal intensities of the aneurysmal sac (SI sac) and paraspinal muscle (SI muscle) using a region-of-interest cursor (1–2 cm^2) on each axial noncontrast MRA. While SI sac values were measured in three areas outside of the stent-graft, SI muscle values were measured in two areas and then averaged. Next, the SIR was evaluated as SI sac divided by the SI muscle. We categorized patients into enlarged (> 5 mm diameter enlargement during observation periods), shrunk (> 5 mm diameter reduction during observation periods), and stable (others) groups based on the size changes in the maximum minor axis diameter of aneurysms assessed by using all the CT images of each patient obtained after EVAR. Furthermore, we assessed the correlation between the SIR and these groups.

Qualitative Analysis

Gold Standard

In this study, 3 unblinded authors reviewed the dual-phase contrast-enhanced CT images of all the patients as the gold standard and reached a consensus on EL identification.

Image Analysis

Before the blinded qualitative analysis, the 3 unblinded authors also reviewed the noncontrast MRA images of all patients and determined the following six possible imaging features of the aneurysmal sac status after EVAR (Fig. 2): 1) mottled high-intensity area, 2) creeping high-intensity area with the low-band rim, 3) crescent-shaped high-intensity area, 4) homogeneous blood sinus cavity, 5) no signal black spot, and 6) layered high-intensity

 https://doi.org/10.3348/kjr.2020.0001

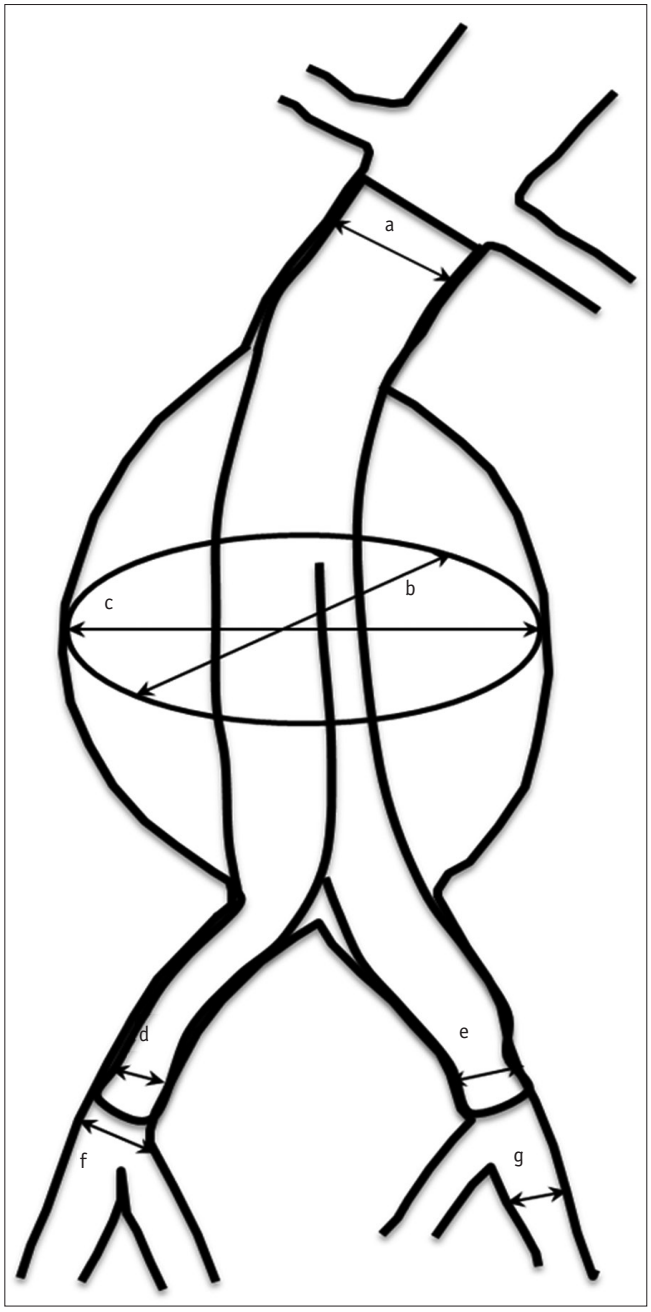

Fig. 1. The diagram shows the measurements of the key anatomical structures for the following aneurysms treated using stent-grafts. a = aortic neck diameter in proximal stent-graft edge, b = maximum minor axis diameter of the aneurysm, c = maximum diameter of the aneurysm, d = right iliac diameters at the distal stent-graft edge, e = left iliac diameters at the distal stent-graft edge, f = right iliac diameters peripheral to the stent-graft edge, g = left iliac diameters peripheral to the stent-graft edge

area. Notably, we evaluated the statistical significance and diagnostic performance of these features in advance of following the blind reading.

Next, the same 2 observers reviewed and assessed all the MRA images for the presence of these features. Moreover, the observers assigned a qualitative rating for the presence of ELs in MRA images using a 5-point scale as follows: 1 = definitely absent, 2 = probably absent, 3 = indeterminate, 4 = probably present, and 5 = definitely present. At the time of review, all the observers were informed that the sensitivities were evaluated using the number of patients allocated a rating of either 4 or 5, whereas the specificities were ascertained using the number of patients with ratings of 1, 2, or 3.

Statistical Analysis

The SPSS for Windows software (version 21.0; IBM Corp.) was used to perform all the statistical analyses.

Anatomical Measurements

We evaluated Pearson's correlation and intraclass correlation coefficients for each measurement to determine intermodality and interobserver differences for evaluating statistical significance. We considered $p < 0.05$ as statistically significant in this study.

Signal Intensity Ratio

We evaluated the SIR as a possible indicator for estimating the prognosis of treated aneurysms on noncontrast MRIs. We used the Kruskal–Wallis test to investigate statistically significant differences in the SIR among the three groups. Furthermore, multiple comparisons were performed in cases displaying statistically significant differences among the three groups.

Qualitative Analysis

We used the Fisher's exact test to correlate the frequencies of MRA features between patients with and without ELs; $p < 0.05$ was considered statistically significant. In addition, a receiver operating characteristic (ROC) curve was fitted to each radiologist's confidence rating for the presence of ELs using a maximum likelihood estimation evaluated using the SPSS software. Furthermore, we estimated the observer performance for each reader by evaluating the area under the ROC curve (AUC). In this study, statistics was applied to determine the degree of agreement in interobserver variability in the image interpretation: up to 0.20 = slight agreement; 0.21–0.40 = fair agreement; 0.41–0.60 = moderate agreement; 0.61–0.80 = substantial agreement; and ≥ 0.81 = almost perfect agreement.

https://doi.org/10.3348/kjr.2020.0001

Korean Journal of Radiology
KJR

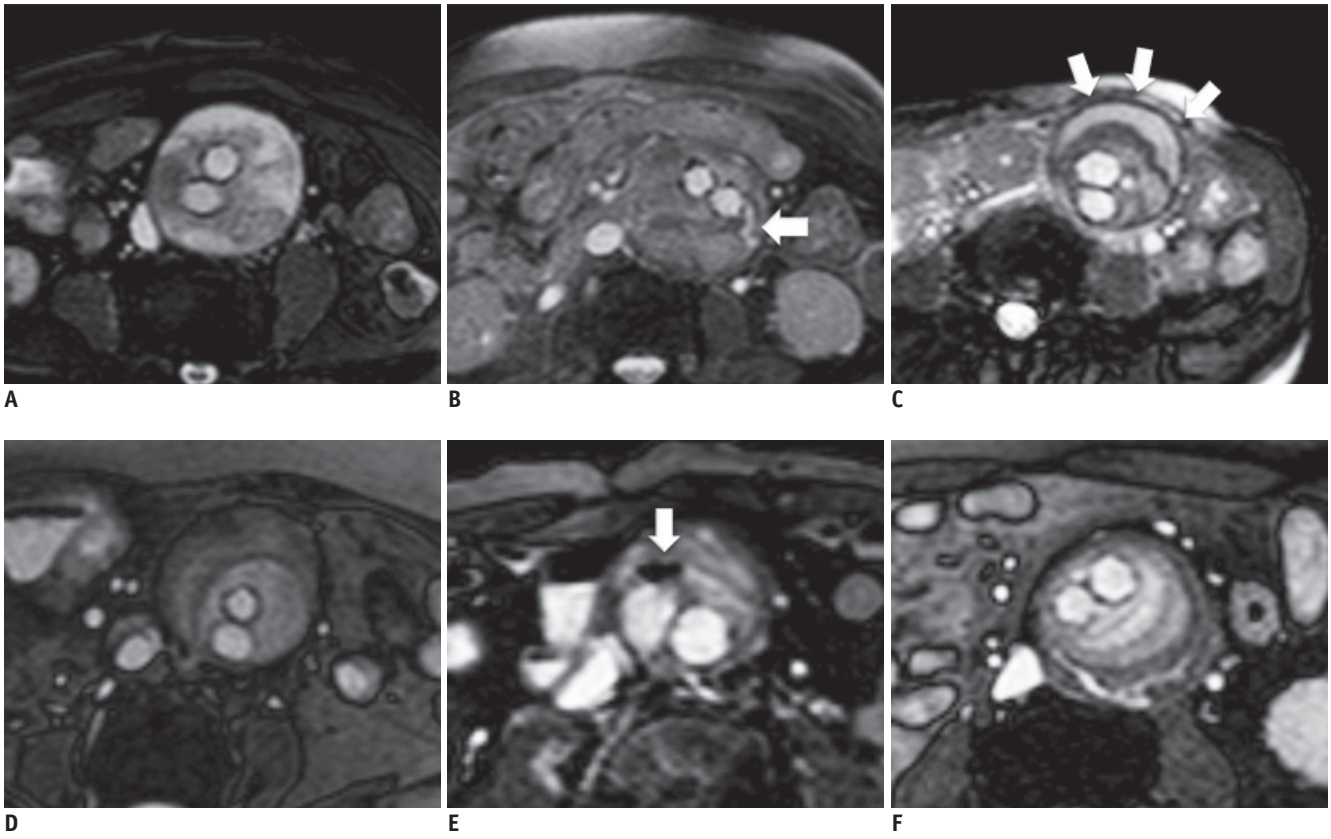

Fig. 2. Samples of the six features examined on noncontrast enhanced single-shot b-TFE MRA.
A. The mottled high-intensity area. **B.** The creeping high-intensity area with the low-band rim (arrow). **C.** The crescent-shaped high-intensity area (arrows). **D.** The homogeneous blood sinus cavity. **E.** No signal black spot (arrow). **F.** The layered high-intensity area. b-TFE MRA = balanced turbo-field-echo magnetic resonance angiography

RESULTS

Phantom Study

When using Zenith stent-grafts, diameter measurements were impossible because of severe metal-induced susceptibility artifacts (Supplementary Fig. 2). We measured the stent-graft diameter of the other three stent-grafts and evaluated the ExRs. The average ExR values of Powerlink (in joint-portion, 136.9%; off-joint-portion, 126.8%) were markedly higher than those of Endurant (111.4%) and Excluder (112.9%). Hence, we only assessed patients treated with Endurant and Excluder stent-grafts in our clinical study.

Clinical Study

Patients

We enrolled 108 patients in this study; however, based on the phantom study results, 26 patients who underwent EVAR using Zenith and Powerlink were excluded from our study cohort because of their severe metallic artifacts. In addition, we excluded 36 patients because of our inability to obtain both contrast-enhanced CTA and noncontrast MRA images. Hence, we analyzed 46 patients (39 males and 7 females; mean age, 76.8 years; age range, 53–91 years) (Fig. 3).

Quantitative Analysis

Anatomical Measurements

Table 1 summarizes vascular measurements, intermodality Pearson's correlation coefficients, and interobserver intraclass correlation coefficients. Vascular measurements obtained using both CTA and MRA images displayed a robust correlation for all the anatomical structures (r = 0.92–0.99; p < 0.001). Furthermore, the interobserver reproducibility of CTA and MRA measurements was excellent for both observers (intraclass correlation coefficient = 0.97–0.99, p < 0.001).

SIR

In this study, the mean observation period after MRA using CT images was 14.2 (range: 3.0–44.5) months.

https://doi.org/10.3348/kjr.2020.0001

We observed no significant differences in the SIR among the three groups (p = 0.65). The SIR values for the enlarged, stable, and shrunk groups were 2.63, 2.47, and 2.48, respectively.

Qualitative Analysis

Gold Standard

We detected ELs in 22 patients; of these, multiple type II ELs were detected in 12 patients. Overall, 41 ELs (type Ia, 2;

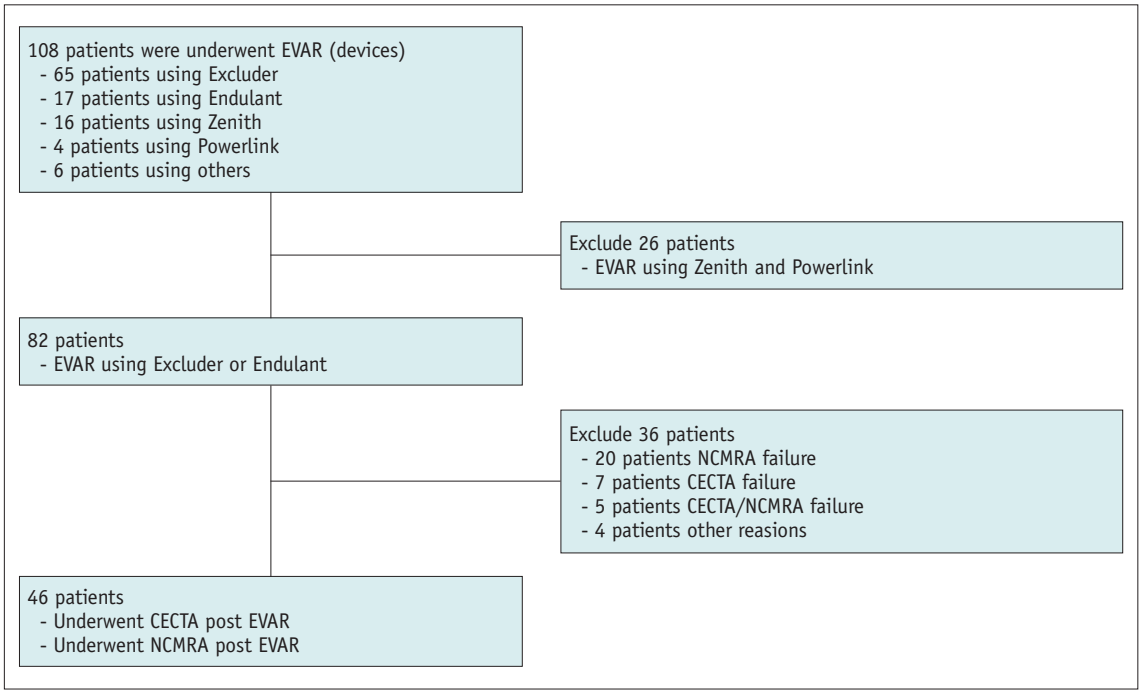

Fig. 3. The flowchart of the study cohort. EVAR = endovascular aneurysm repair

Table 1. Vascular Measurements and Statistical Results for Anatomical Structures with CTA and b-TFE MRA

Anatomical Structures	Observer 1			Observer 2			Observers 1 vs. 2	Observers 1 vs. 2
	CTA	MRA	*r*	CTA	MRA	*r*	ICC for CTA	ICC for MRA
Aortic neck diameter in stent-graft	18.5 ± 3.0 (9.7–25.5)	18.6 ± 3.0 (10.1–25.5)	0.99	18.1 ± 3.0 (9.7–25.3)	18.8 ± 3.2 (10.1–26.5)	0.92	0.98	0.97
Maximum minor axis diameter of the aneurysm	51.3 ± 8.9 (31.5–74.3)	51.3 ± 8.8 (31.8–74.1)	0.99	50.6 ± 8.9 (29.3–73.7)	51.5 ± 8.9 (30.9–76.6)	0.96	0.99	0.98
Maximum diameter of the aneurysm	50.2 ± 21.7 (0.0–82.8)	51.1 ± 20.6 (0.0–82.8)	0.99	56.3 ± 10.1 (0.0–81.2)	57.7 ± 10.3 (0.0–82.6)	0.96	0.99	0.98
Right iliac diameters in stent-graft	11.4 ± 3.3 (0.0–19.9)	11.5 ± 3.4 (0.0–20.3)	0.99	11.4 ± 3.0 (0.0–18.5)	11.8 ± 3.1 (0.0–20.4)	0.95	0.98	0.98
Left iliac diameters in stent-graft	11.8 ± 3.3 (6.1–19.1)	11.8 ± 3.2 (6.0–19.4)	0.99	11.6 ± 3.3 (5.2–19.4)	11.9 ± 3.3 (5.3–20.3)	0.94	0.99	0.98
Right iliac diameters more peripheral than a stent-graft edge	10.9 ± 3.0 (6.1–22.4)	10.9 ± 3.0 (6.0–22.3)	0.98	10.7 ± 2.9 (5.6–21.5)	10.4 ± 2.8 (6.0–20.3)	0.94	0.99	0.97
Left iliac diameters more peripheral than a stent-graft edge	10.8 ± 3.2 (6.2–22.0)	10.9 ± 3.2 (6.3–22.1)	0.99	10.5 ± 3.4 (6.2–21.9)	10.5 ± 3.0 (6.0–20.3)	0.95	0.99	0.97

Data are mean (mm) ± 1 standard deviation. Numbers in parentheses are ranges. b-TFE MRA = balanced turbo-field-echo magnetic resonance angiography, CTA = computed tomography angiography, ICC = intraclass correlation coefficient between observers, MRA = magnetic resonance angiography, *r* = Pearson's correlation coefficient between CTA and MRA

https://doi.org/10.3348/kjr.2020.0001

Korean Journal of Radiology
KJR

type II, 39) were detected in these patients.

Image Analysis

Table 2 summarizes the frequencies of MRA features identified by unblinded authors. We observed significant differences in frequency between patients with and without ELs for the "mottled high-intensity area" (p = 0.001), "creeping high-intensity area with the low-band rim" (p < 0.001), "no signal black spot" (p = 0.031), and "layered high-intensity area" (p = 0.003). While the "creeping high-intensity area with the low-band rim" (63.6%) (Fig. 4) and "mottled high-intensity area" (45.5%) (Fig. 5) were often observed in patients with ELs and considered positive, "no signal black spot" (20.8%) (Fig. 6) and "layered high-intensity area" (41.7%) (Fig. 5) were often observed in patients without ELs and considered negative. In addition, we observed no significant differences in other features. Table 3 summarizes the sensitivity, specificity, and accuracy of all positive and negative MRA features. If one of the two positive features was noted, the sensitivity, specificity, and accuracy for the presence of ELs were 77.3%, 91.7%, and 84.8%, respectively. If one of the two negative features was observed, the sensitivity, specificity, and accuracy were 95.5%, 50.0%, and 71.7%, respectively.

Table 4 summarizes the frequencies of MRA features identified by the observers in the review. Both observers precisely detected the frequencies of positive and negative features. The sensitivity, specificity, and AUC for the detection of ELs as evaluated by observer 1 were 72.7%, 87.5%, and 0.82, respectively, whereas those for observer 2, were 63.6%, 70.8%, and 0.71, respectively (Supplementary Fig. 3). In addition, the κ values between unblinded

Table 2. Frequencies of MRA Features in Patients with or without EL by Unblinded Authors' Review

MRA Features	With EL (n = 22)	Without EL (n = 24)	*P*
Mottled high intensity area*	10 (45.5)	1 (4.3)	0.001
Creeping high intensity area with low band rim*	14 (63.6)	1 (4.3)	< 0.001
Crescent-shaped high intensity area	4 (18.2)	9 (37.5)	0.130
Homogeneous blood sinus cavity	5 (22.7)	8 (33.3)	0.320
No signal black spot*	0 (0.0)	5 (20.8)	0.031
Layered high intensity area*	1 (4.5)	10 (41.7)	0.003

Numbers in parentheses are percentages. Data are presented as numbers of patients. *Difference between the two groups of patients was statistically significant. EL = endoleak

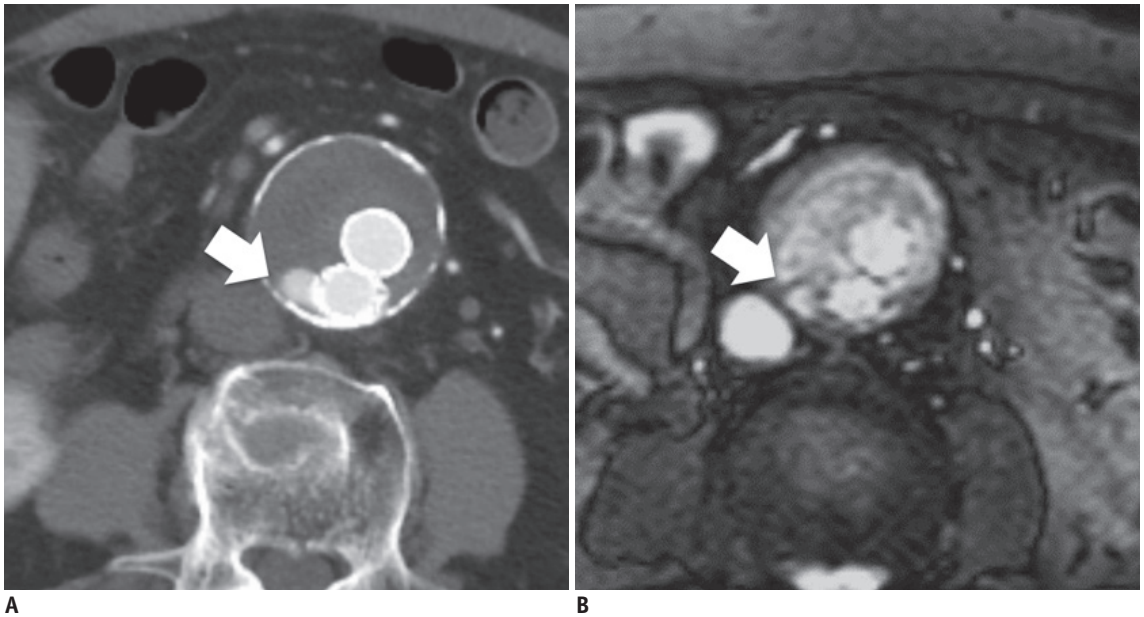

Fig. 4. A 69-year-old male with an infrarenal aortic aneurysm treated by EVAR.
A. A transaxial contrast-enhanced CT image demonstrates a well-defined blood cavity due to type II endoleak from the lumber artery (arrow). **B.** A transaxial noncontrast single-shot b-TFE MRA demonstrates a "creeping high-intensity area with the low-band rim" corresponding to the type II endoleaks detected in the image **(A)** (arrow). CT = computed tomography

https://doi.org/10.3348/kjr.2020.0001

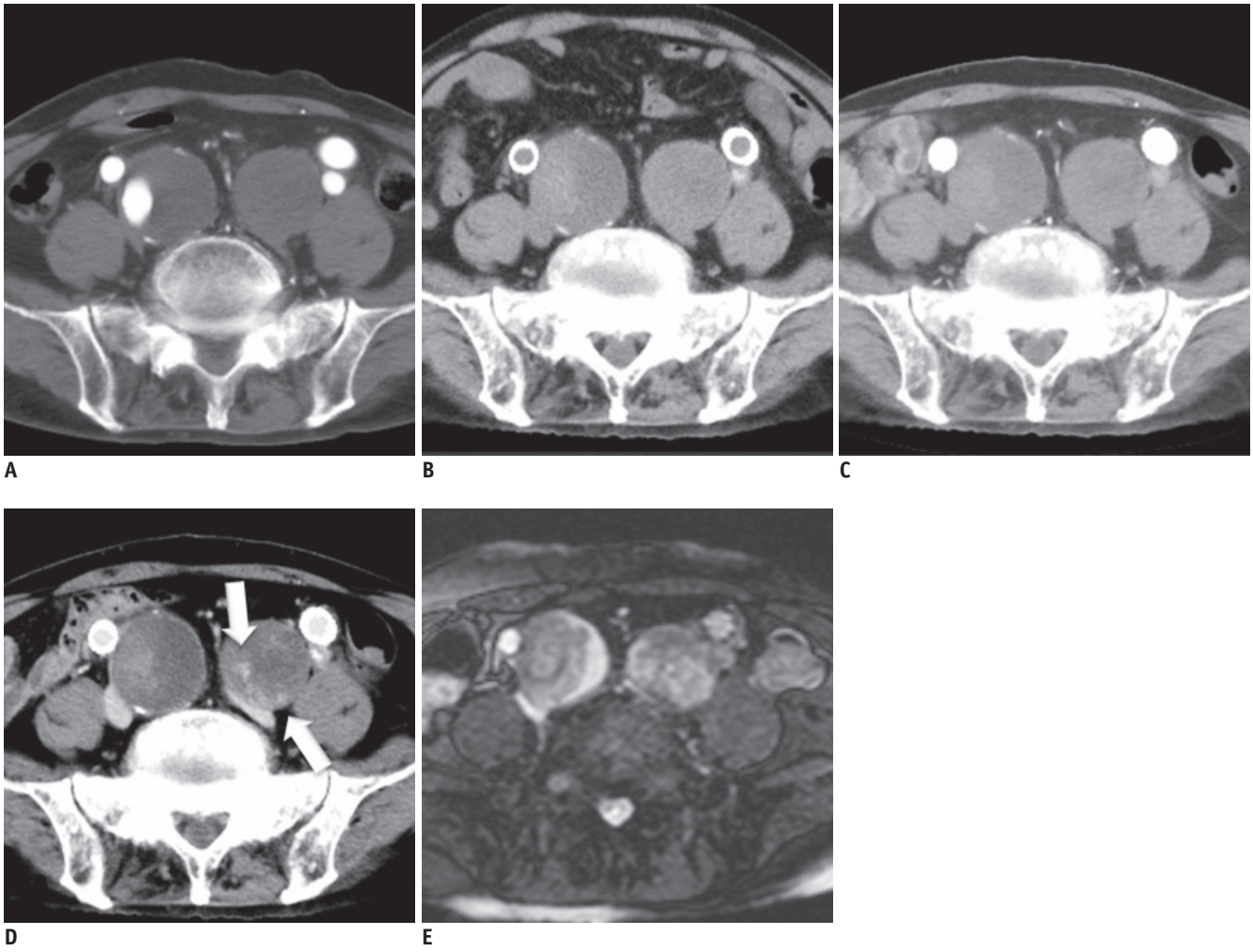

Fig. 5. Images of a 77-year-old male with an infrarenal aortic and both common iliac artery aneurysms treated by EVAR.
A. An axial image obtained using contrast-enhanced CTA before treatment. **B-D.** Axial images obtained using noncontrast **(B)** and contrast-enhanced CTA **(C, D)**. A type II endoleak in the left common iliac artery was only observed in the delayed phase (arrows). **E.** An axial image obtained using a single-shot b-TFE sequence as a noncontrast-enhanced MRA. The "mottled high-intensity area" was observed in the left common iliac artery and "layered high-intensity area" was observed in the right common iliac artery. CTA = computed tomography angiography

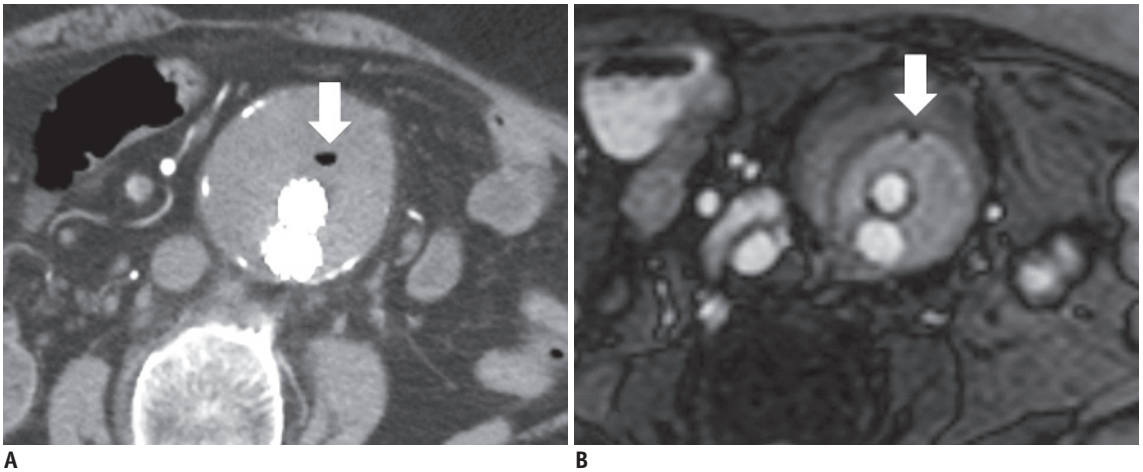

Fig. 6. Images of a 75-year-old female with an infrarenal aortic aneurysm.
A. An axial image obtained using contrast-enhanced CTA with air density within an aneurysmal sac (arrow). **B.** An axial image obtained using noncontrast-enhanced MRA with "no signal black spot" (arrow).

https://doi.org/10.3348/kjr.2020.0001

Korean Journal of Radiology
KJR

Table 3. Sensitivity and Specificity of Positive and Negative MRA Features for the Diagnosis of ELs

MRA Features	Sensitivity	Specificity	PPV	NPV	Accuracy
Positive features					
Mottled high intensity area	45.5	95.8	90.9	65.7	71.7
Creeping high intensity area with low band rim	63.6	95.8	93.3	74.2	80.4
One of them	77.3	91.7	89.5	81.5	84.8
Both of them	31.8	100	100	61.5	67.4
Negative features					
No signal black spot	100	20.8	53.7	100	58.7
Layered high intensity area	95.5	41.7	60.0	90.9	67.4
One of them	95.5	50.0	63.6	92.3	71.7
Both of them	100	12.5	51.2	100	54.3

These values are percentages. NPV = negative predictive value, PPV = positive predictive value

Table 4. Frequencies of MRA Features in Patients with or without EL by Observers' Review

MRA Features	With EL (n = 22)		Without EL (n = 24)	
	Observer 1	Observer 2	Observer 1	Observer 2
Mottled high intensity area*	10 (45.5)	9 (40.9)	1 (4.3)	2 (8.3)
Creeping high intensity area with low band rim*	13 (51.9)	10 (45.5)	3 (12.5)	2 (8.3)
No signal black spot*	0 (0.0)	0 (0.0)	7 (29.2)	5 (20.8)
Layered high intensity area	1 (4.5)	6 (27.3)	10 (41.7)	11 (45.8)

Numbers in parentheses are percentages. Data are presented as numbers of patients. *Difference between the two groups of patients was statistically significant ($p < 0.05$) in observer 1 and observer 2.

authors and observers or interobservers were 0.40–0.88, exhibiting moderate to almost perfect levels of agreement.

DISCUSSION

The EUROSTAR registry reported that ELs, migration, and kinking markedly correlated with the late rupture of treated aneurysms (7). Although post-EVAR follow-up imaging is essential to identify EVAR-related complications (17), accrued radiation exposure and the potential for nephrotoxicity due to contrast-enhanced CT remain a concern (18). Although gadolinium-enhanced MRA is at least as sensitive as CTA (19-21), nephrogenic systemic fibrosis has become a concern in patients with chronic kidney disease (22, 23). Reportedly, patients with AAA are relatively older and often experience chronic renal failure (24); thus, the use of gadolinium-based contrast materials should be discouraged in these patients who might need recurrent examinations during the pre- and/or post-treatment period. Although duplex ultrasound and contrast-enhanced ultrasound are potential substitutes to CTA or MRA, ultrasound has disadvantages, such as operator dependence and variability in the image quality based on patients' body habitus (18). Hence, in this study, we used a noncontrast b-TFE sequence because of its excellent contrast resolution (25). A previous study established the adequacy of b-TFE in offering the required anatomical information for preoperative EVAR planning (12). Likewise, this study also demonstrates that measurements obtained using CTA and noncontrast b-TFE MRA exhibit excellent intermodality and interobserver agreement despite the presence of stent-graft-induced susceptibility artifacts.

Moreover, b-TFE MRA exhibits excellent contrast for the aortic lumen where the blood flows in the stent-graft, mural thrombus mixed with old and new blood clots, and aortic walls comprising smooth muscles and collagenous fibers. Thus, we determined the presence of four b-TFE MRA features that possibly correlated with the presence of ELs. Regarding two positive features, we assume that a "creeping high-intensity area with the low-band rim" depicts blood inflow to the aneurysmal sac with a fibrin pseudomembrane, which probably signifies ELs with a certain flow rate noted as a well-defined blood sinus cavity in the early phase of contrast-enhanced CTA. Perhaps, a "mottled high-intensity area" is the result of the slow blood flow spread in a closed aneurysmal sac, which was noticed in the delayed phase of contrast-enhanced CTA. Regarding two negative features, we assume that "no signal black spot" signifies the air trapped within a sac during stent-graft procedures, which was also noted by contrast-enhanced CTA. In addition, we

 https://doi.org/10.3348/kjr.2020.0001

consider that the aneurysmal sac is impeccably excluded from the systemic circulation without ELs. Furthermore, a "layered high-intensity area" could be the result of stepwise and layered clotting in the excluded aneurysmal sac.

Reportedly, the clot formation in excluded aneurysmal sacs accounts for declined SIs in T2-weighted images (26, 27). Thus, layered T2 value changes could be observed during the clot formation process within the excluded aneurysmal sac. In addition, this study illustrated characteristic b-TFE MRA features that comprise mixed high- and low- intensities at various degrees and patterns that might depend on EL flow rates and the clot formation process within treated sacs. Moreover, we considered that the SIR assumedly signifies the moisture content and clot formation degree within the excluded aneurysmal sac, which could affect the aneurysm prognosis after the EVAR treatment. However, we observed no marked correlation between the SIR and prognosis. Reportedly, noncontrast b-TFE MRA is inferior to contrast-enhanced CTA or MRA for the visualization of peripheral vessels or microstructures (28). Hence, contrast-enhanced CTA or MRA should be used for detecting EL culprit vessels in alleged cases based on the noncontrast MRA assessment.

This study has several limitations that should be acknowledged. First, although we empirically considered CTA to be the reference standard, some studies have indicated that contrast-enhanced MRI is markedly more sensitive than CT for the detection of ELs (29, 30). Second, no patient in our cohort had type III, IV, or V ELs, which could be held accountable for variable flow rates and patterns in this study. Thus, further clinical trials are warranted to establish the diagnostic performance of our technique for these ELs. Third, we obtained MRA images only within 2 weeks after EVAR. In the early postoperative period, various factors, such as acute hemorrhage, are involved in the signal in the aneurysmal sac, which are likely to be confounded with ELs. These factors may lead to the moderate sensitivity of our technique for the detection of ELs. Thus, further clinical studies are needed to validate the diagnostic performance of noncontrast MRA obtained in the late postoperative period. Finally, our findings are limited by the utility of b-TFE MRA to selected stent-grafts because of the presence of unavoidable metallic artifacts. Furthermore, contraindications of MRI, such as claustrophobia, some other types of metal implants, and the presence of implanted pacemakers, limited our sample size. Given the development of MR-conditional pacemakers (31, 32), a similar cross-sectional survey of a large EVAR-treated cohort is warranted to ascertain the possible expanded adoption of MRI.

In conclusion, this study reveals that the use of noncontrast b-TFE MRA without ionizing radiation or contrast media offers an adequate depiction of EVAR-treated aortic lumen. Furthermore, these images enable the precise measurements of anatomical structures and the identification of high-risk patients suspected to have ELs.

Supplementary Materials

The Data Supplement is available with this article at https://doi.org/10.3348/kjr.2020.0001.

Conflicts of Interest

The authors have no potential conflicts of interest to disclose.

ORCID iDs

Hiroshi Kawada
https://orcid.org/0000-0001-8613-2044
Satoshi Goshima
https://orcid.org/0000-0002-1897-5709
Yoshifumi Noda
https://orcid.org/0000-0003-3611-4790
Kimihiro Kajita
https://orcid.org/0000-0002-3512-4981
Yukichi Tanahashi
https://orcid.org/0000-0003-1602-9396
Nobuyuki Kawai
https://orcid.org/0000-0002-7900-026X
Narihiro Ishida
https://orcid.org/0000-0002-3741-8553
Masayuki Matsuo
https://orcid.org/0000-0001-7615-3247

REFERENCES

1. Greenhalgh RM, Brown LC, Kwong GP, Powell JT, Thompson SG; EVAR trial participants. Comparison of endovascular aneurysm repair with open repair in patients with abdominal aortic aneurysm (EVAR trial 1), 30-day operative mortality results: randomised controlled trial. *Lancet* 2004;364:843-848
2. United Kingdom EVAR Trial Investigators, Greenhalgh RM, Brown LC, Powell JT, Thompson SG, Epstein D, et al. Endovascular versus open repair of abdominal aortic aneurysm. *N Engl J Med* 2010;362:1863-1871

3. De Bruin JL, Baas AF, Buth J, Prinssen M, Verhoeven EL, Cuypers PW, et al. Long-term outcome of open or endovascular repair of abdominal aortic aneurysm. *N Engl J Med* 2010;362:1881-1889
4. Albuquerque FC Jr, Tonnessen BH, Noll RE Jr, Cires G, Kim JK, Sternbergh WC 3rd. Paradigm shifts in the treatment of abdominal aortic aneurysm: trends in 721 patients between 1996 and 2008. *J Vasc Surg* 2010;51:1348-1353
5. Ilyas S, Shaida N, Thakor AS, Winterbottom A, Cousins C. Endovascular aneurysm repair (EVAR) follow-up imaging: the assessment and treatment of common postoperative complications. *Clin Radiol* 2015;70:183-196
6. Picel AC, Kansal N. Essentials of endovascular abdominal aortic aneurysm repair imaging: postprocedure surveillance and complications. *AJR Am J Roentgenol* 2014;203:W358-W372
7. Fransen GA, Vallabhaneni SR Sr, van Marrewijk CJ, Laheij RJ, Harris PL, Buth J, et al. Rupture of infra-renal aortic aneurysm after endovascular repair: a series from EUROSTAR registry. *Eur J Vasc Endovasc Surg* 2003;26:487-493
8. Chaikof EL, Brewster DC, Dalman RL, Makaroun MS, Illig KA, Sicard GA, et al. SVS practice guidelines for the care of patients with an abdominal aortic aneurysm: executive summary. *J Vasc Surg* 2009;50:880-896
9. Walker TG, Kalva SP, Yeddula K, Wicky S, Kundu S, Drescher P, et al. Clinical practice guidelines for endovascular abdominal aortic aneurysm repair: written by the standards of practice committee for the society of interventional radiology and endorsed by the cardiovascular and interventional radiological society of europe and the canadian interventional radiology association. *J Vasc Interv Radiol* 2010;21:1632-1655
10. Moll FL, Powell JT, Fraedrich G, Verzini F, Haulon S, Waltham M, et al. Management of abdominal aortic aneurysms clinical practice guidelines of the European society for vascular surgery. *Eur J Vasc Endovasc Surg* 2011;41 Suppl 1:S1-S58
11. Stavropoulos SW, Charagundla SR. Imaging techniques for detection and management of endoleaks after endovascular aortic aneurysm repair. *Radiology* 2007;243:641-655
12. Goshima S, Kanematsu M, Kondo H, Kawada H, Kojima T, Sakurai K, et al. Preoperative planning for endovascular aortic repair of abdominal aortic aneurysms: feasibility of nonenhanced MR angiography versus contrast-enhanced CT angiography. *Radiology* 2013;267:948-955
13. Salehi Ravesh M, Langguth P, Pfarr JA, Schupp J, Trentmann J, Koktzoglou I, et al. Non-contrast-enhanced magnetic resonance imaging for visualization and quantification of endovascular aortic prosthesis, their endoleaks and aneurysm sacs at 1.5T. *Magn Reson Imaging* 2019;60:164-172
14. Bae KT. Peak contrast enhancement in CT and MR angiography: when does it occur and why? Pharmacokinetic study in a porcine model. *Radiology* 2003;227:809-816
15. Kanematsu M, Goshima S, Miyoshi T, Kondo H, Watanabe H, Noda Y, et al. Whole-body CT angiography with low tube voltage and low-concentration contrast material to reduce radiation dose and iodine load. *AJR Am J Roentgenol* 2014;202:W106-W116
16. Tanahashi Y, Goshima S, Kondo H, Noda Y, Sakurai K, Kawada H, et al. Additional value of venous phase added to aortic CT angiography in patients with aortic aneurysm. *Clin Imaging* 2017;44:51-56
17. Patel A, Edwards R, Chandramohan S. Surveillance of patients post-endovascular abdominal aortic aneurysm repair (EVAR). A web-based survey of practice in the UK. *Clin Radiol* 2013;68:580-587
18. Tse DM, Tapping CR, Patel R, Morgan R, Bratby MJ, Anthony S, et al. Surveillance after endovascular abdominal aortic aneurysm repair. *Cardiovasc Intervent Radiol* 2014;37:875-888
19. Ayuso JR, de Caralt TM, Pages M, Riambau V, Ayuso C, Sanchez M, et al. MRA is useful as a follow-up technique after endovascular repair of aortic aneurysms with nitinol endoprostheses. *J Magn Reson Imaging* 2004;20:803-810
20. Pitton MB, Schweitzer H, Herber S, Schmiedt W, Neufang A, Kalden P, et al. MRI versus helical CT for endoleak detection after endovascular aneurysm repair. *AJR Am J Roentgenol* 2005;185:1275-1281
21. van der Laan MJ, Bartels LW, Viergever MA, Blankensteijn JD. Computed tomography versus magnetic resonance imaging of endoleaks after EVAR. *Eur J Vasc Endovasc Surg* 2006;32:361-365
22. Cowper SE, Robin HS, Steinberg SM, Su LD, Gupta S, LeBoit PE. Scleromyxoedema-like cutaneous diseases in renal-dialysis patients. *Lancet* 2000;356:1000-1001
23. Kuo PH, Kanal E, Abu-Alfa AK, Cowper SE. Gadolinium-based MR contrast agents and nephrogenic systemic fibrosis. *Radiology* 2007;242:647-649
24. Hagiwara S, Saima S, Negishi K, Takeda R, Miyauchi N, Akiyama Y, et al. High incidence of renal failure in patients with aortic aneurysms. *Nephrol Dial Transplant* 2007;22:1361-1368
25. Miyazaki M, Isoda H. Non-contrast-enhanced MR angiography of the abdomen. *Eur J Radiol* 2011;80:9-23
26. Engellau L, Larsson EM, Albrechtsson U, Jonung T, Ribbe E, Thörne J, et al. Magnetic resonance imaging and MR angiography of endoluminally treated abdominal aortic aneurysms. *Eur J Vasc Endovasc Surg* 1998;15:212-219
27. Pitton MB, Schmenger RP, Neufang A, Konerding MA, Düber C, Thelen M. Endovascular aneurysm repair: magnetic resonance monitoring of histological organization processes in the excluded aneurysm. *Circulation* 2002;105:1995-1999
28. Herborn CU, Watkins DM, Runge VM, Gendron JM, Montgomery ML, Naul LG. Renal arteries: comparison of steady-state free precession MR angiography and contrast-enhanced MR angiography. *Radiology* 2006;239:263-268
29. Haulon S, Lions C, McFadden EP, Koussa M, Gaxotte V, Halna P, et al. Prospective evaluation of magnetic resonance imaging after endovascular treatment of infrarenal aortic aneurysms. *Eur J Vasc Endovasc Surg* 2001;22:62-69
30. Habets J, Zandvoort HJ, Reitsma JB, Bartels LW, Moll FL, Leiner T, et al. Magnetic resonance imaging is more sensitive

 https://doi.org/10.3348/kjr.2020.0001

than computed tomography angiography for the detection of endoleaks after endovascular abdominal aortic aneurysm repair: a systematic review. *Eur J Vasc Endovasc Surg* 2013;45:340-350
31. Wollmann CG, Thudt K, Kaiser B, Salomonowitz E, Mayr H, Globits S. Safe performance of magnetic resonance of the heart in patients with magnetic resonance conditional pacemaker systems: the safety issue of the ESTIMATE study. *J Cardiovasc Magn Reson* 2014;16:30
32. Kaasalainen T, Pakarinen S, Kivisto S, Holmstrom M, Hänninen H, Peltonen J, et al. MRI with cardiac pacing devices - safety in clinical practice. *Eur J Radiol* 2014;83:1387-1395

https://doi.org/10.3348/kjr.2020.0001